Author version: *Mar. Pet. Geol., vol.29; 2012; 115-128*

Characterization of seafloor pockmark seepage of hydrocarbons employing fractal: A case study from the Western Continental Margin of India

Sumanta Dandapath[1,*], Bishwajit Chakraborty[1,**],Nicolas Maslov[1, 2,***], Siddaiah M. Karisiddaiah[1], Dhrupad Ghosh[1], William Fernandes[1] and Andrew Menezes[1]

[1]*National Institute of Oceanography, Council of Scientific and Industrial Research, Dona Paula, Goa - 403 004, India*

[2] *Master Recherche, IRENav, Arts et Metiers ParisTech, 151, bd de l'Hopital 75013 Paris, France*

** Presently at Shivaji University, Kolhapur - 416004, India*

** Corresponding author.
Tel.: +91-832-2450-318; Fax: +91-832-2450-602.
Email: bishwajit@nio.org (B. Chakraborty).

**** Internship at NIO, Goa.*

Abstract

Here we apply quantitative technique to describe the seafloor seepages based on the multibeam backscatter and bathymetric investigations to characterize the pockmark morphology. The variable seafloor backscatter strength for coarser seafloor sediments are related to the diagenesis derived from biodegraded seepages. In this regard, box counting method is used to estimate 'fractal dimension' for backscatter imagery data of 398 blocks. These blocks are further sub-grouped into six classes depending on the spread of pockmark related seepages. The study area lies 102 km west off Marmagao along the central west coast of India which contains pre-dominantly (70%) gas-charged sediments. Comparison between the estimated self similar fractals reveals that there is approximately 97% correlation between the box (D_{box}) and information (D_{info}) dimensions. Box dimension-derived fractal dimension values suggest that the seepages are more along the fault trace in deeper waters, in comparison to sparsely distributed shallow water seepages. Besides, this poor seepage is confined within the smooth to moderately rough seafloor. It is established that the high backscatter strength along the upper slope of the pockmark region having higher fractal dimensions reflects multifractal behavior of seepage distribution. Entire area indicates patchy seepage patterns as supported by estimated fractal values showing intermittent fluctuations, which emphasizes non-linear behavior. Estimated self organizing criticality (SOC) parameters for six representative blocks reveal that the nature of pockmark, fault trace, sediment nature coupled with slumping of pockmark's wall, sediment movement due to bottom currents are controlling the dynamic balance in the area seepage system. Further, our study emphasizing the multifractal behavior of seepage blocks, clearly depicts the drift in the seepage pattern.

Keywords: *Seafloor seepage characterization, Multibeam bathymetry and backscatter image, Fractal dimension, Box counting method, Acoustic remote sensing, Central west coast of India, off Marmagao, Self organizing criticality, Multifractal*

1. Introduction

Seafloor seepages, being one of the most potential energy resources offer important proxy for shallow or deep hydrocarbon accumulations. Pockmark associated seepages (King and MacLean, 1970) are prevalent from sub-arctic to tropical seas, continental shelf to deep ocean basins, even in shallow deep lakes under different geological environments. Parameters such as gas or fluids, nature of migration pathways (e.g., fault, diapir etc), permeability of sub-surface sediments, and sediment grain sizes are important to ascertain the seafloor seepage type (Paull et al., 2002; Hovland et al., 2005; Chand et al., 2009). Seafloor seepage characterization is one of the major concerns towards the understanding of the fluid flow processes (Abrams, 1996).

Generally, higher acoustic backscatter strengths in the pockmark zone suggest coarser sediment, which is linked to the precipitation of diagenitic minerals from the biodegradation of seepage material (Wen and Sinding-Larsen, 1996; Loncke and Mascle, 2004; Logan et al., 2010). Such backscatter variability is also functional to the seafloor slope, sediment type and relief (Blondel, 2009). Recently, using multibeam bathymetry and backscatter data semi-quantitative study of the morphological aspects of the pockmarks were carried out (Dandapath et al., 2010). Fault-controlled pockmarks in the study area are observed to be associated with the fluid escape features in the form of seeps. This fault zone is considered to be connected with the BSRs located in the slope region (Fig. 1a), and resultant gas/fluids emanated to the surface might lead to the formation of pockmarks (Fig. 1b) (Andrews et al., 2010), which probably may reworked by combined effects of bottom currents and submarine slumping. Main objective of the present study is to develop a quantitative understanding of the seafloor seepage morphology utilizing backscatter imagery, which ought to provide an indirect indication for hydrocarbon accumulations.

Seafloor roughness was studied in the past using fractal dimension parameter of the depth and backscatter images (Fox and Hayes, 1985). The fractal dimension is used to measure the degree of fragmentation and irregularities linked to the behavior of the system (Mandelbrot, 1977; Mandelbrot, 1983). Monofractals are homogeneous objects having same scaling properties, and characterized by a single singularity exponent (Stanley et al., 1999). But many of the fractals observed in nature have infinite hierarchy of statistical exponents that offer a convenient framework to quantify the complex systems (Dimri, 2005). Therefore, processes cannot be said monofractal for more complicated cases where different scaling exponents can be revealed for many interwoven fractal subsets of time series, and such processes are recognized as multifractals (Telesca et al., 2002).

It is pertinent to refer here the application of the statistical analyses of the patch patterns e.g., microphytobenthos from intertidal areas (Seuront and Spilmont, 2002) and deep continental margins (Beyer et al., 2007) which indicate fractal and multifractal structures following specific power law behavior. In this study, similar investigations were adapted for patchy intermittent pockmarks seepage patterns (spatial heterogeneity in terms of backscatter strength), which addresses significance of inherent intermittency characterizing the seafloor seepages at different scales. Understanding the origin of the intermittent fluctuations in non-equilibrium systems is known as "self organized criticality" (SOC). SOC can be described using fractal object due to their intrinsic scaling properties (Bak et al., 1987). Different scales are related to the backscatter strengths, and fractals can be employed for the detection and characterization of the seepages. In this work, employing remotely acquired multibeam swath bathymetric and backscatter imagery data, understanding of the seafloor seepage related processes are made along the central part of the western continental margin of India (off Goa) (Fig. 1a).

Present communication deals with the quantitative parameter estimation using multibeam backscatter image samples for seafloor seepage morphological studies. We describe here, the application of fractal based techniques to detect and characterize the seafloor seepages using box (Longley and Batty, 1989) and information dimensions (Seuront, 2010) to backscatter images. We also explained seep characteristics of the study area which are linked with the morphology of the associated topography. Our study further shows the relation between the probability distribution of patch/seepages with respect to the seepage concentrations towards the understanding of their SOC. Furthermore, in order to characterize the seepage processes we have dwelt on their inherent multifractality aspects.

2. Materials and methods

2.1 Study area description

Tectonically western continental margin of India is a passive and divergent margin. NNW to SSE trending faults, fractures and ridge system has dissected the area (Chakraborty et al., 2006; Mukhopadhyay et al., 2008). Sediment cover is up to 4 km thick with a higher proportion of total organic carbon (2-4%) having marine origin (Calvert et al., 1995). Present study area is located in the shelf-slope margin within 145-330m water depth, and lies 102 km west off Marmagao along the central west coast of India (Dandapath et al., 2010) (Fig. 1a and b). Calcium carbonate content in the surface sediments (Thamban et al., 1997) is also higher (>60%). Average slope of the seafloor is moderate (0.9˚), however, it become steeper (up to 2˚) in the seaward side. Regional oceanic

circulations characterized by seasonal reversal of monsoon driven surface and bottom currents, summer upwelling and winter down welling (Naqvi et al., 2010), create an unstable oceanographic condition over the area. Bottom currents are wide (~40 km) and runs opposite to the direction of surface currents (Shetye et al., 1990). Average current values toward the deeper part of the study area is measured using mooring systems, which comprised of mean speed and directions. At the commencement of the south-west monsoon, mean speed and directions are 12.6 cm/sec and 94.5 degree respectively. Similarly, during the north-east monsoon, the mean current speed and directions measured in this area are 12.5 cm/sec. and 296.6 degree respectively (Shenoy & Antony, 1991). Seafloor pockmarks, bottom simulating reflectors (BSRs), acoustic blanking, and gas charged sediments are detected during the geological and geophysical surveys (Karisiddaiah and Veerayya, 1994; Satyavani et al., 2005; Dewangan and Ramprasad, 2007). In general, the sediment sample data acquired using Van-veen grab (Sagar Sukti cruise no. 168) show association of abundant shell components. In this area, "clayey sand" and "sandy" sediment types are observed to be associated with the moderate to abundant shell materials. Moreover, in some locations "sandy" sediment without shell materials are also seen.

2.2 Area pockmark formation –a general perception

Sediment cores collected from nearby region suggest high organic carbon in the sediment is preserved by the Oxygen Minimum Zone (anoxic condition) for nearly 450 kyr (Ziegler et al., 2010). Such condition leads to form type II Kerogen (higher proportion of hydrogen), which might provide excellent potential as a hydrocarbon source (Paropkari et al., 1993). Such gases (e.g., methane etc.) might have trapped in the shallow sediment since their origin, or may have migrated through the weaker section of the rock column and then blocked by the impervious layer. Subsequently, during minor tectonic events (e.g., fault in this case) gas/fluid extruded to the surface through seeps and formed pockmarks (Rollet et al., 2009). Gas charged sediments noticed here appear as anomalous signature of the backscatter images (Karisiddaiah and Veerayya, 1994). Association of small mound with the pockmark suggests that gas/fluid is perhaps migrated towards the mound. After due course of time, pressure builds-up and increased in pressure lead to an outbreak through weaker sections (which normally correspond to the seaward side). Through this process, gas expulsion took place and pockmarks are formed and the pathways are vacated after the release of such gases. However some gases are stored in the pore spaces of the sub-surface sediments especially in the upslope side (due to gravitational pull-up). They could not able to either released through the pockmarks, and neither able to build-up enough pressure to form another outbreak due to cut-off supply of gas. Stored gases in the upslope side thus might have formed as small mounds. Expulsion may be repeated through the

same openings (pockmark/seep) following another supply of gas or might have routed through a new openings nearby the earlier one causing formation of complex pockmarks (Yun et al., 1999). Gas stored upslope side and beneath the small mounds may be causing high backscatter and apparently help to map the seepages.

2.3 Backscatter data

The multibeam survey was conducted during November, 2006 by the National Institute of Oceanography (NIO) onboard Coastal Research Vessel (CRV) Sagar Sukti (cruise no.118). Backscatter imagery and bathymetry data for present study was acquired using Kongsberg EM 1002 multibeam echo-sounder operating at 95 kHz frequency. (resolution ????…) Acoustic backscatter imagery and swath bathymetric survey of nearly ~105 km^2 area revealed 112 pockmarks. For details of the pockmarks, please refer Dandapath et al., (2010). Post processing corrections include the removal of tide effects and depth outliers, and gridding of the bathymetric data (Mitchell, 1991). PROcessing BAckscatter SIgnal II (PROBASI II) – an algorithm was used for the corrections of the raw backscatter data (Fernandes and Chakraborty, 2009). The geo-referenced data points, containing backscatter strength (dB) and depth values (m) are imported to ArcGIS. The data were then interpolated to raster using cubic convolution methods and subsequently high resolution image with distinct color scheme was generated. Bathymetric contours at different intervals were superimposed over the backscatter map. Based on the shape and alignment of the bathymetric contours, morphological features such as depression/pockmarks, fault, small mounds etc. were identified (Fig. 1b). With the help of the combined map of the backscatter and bathymetry, the seep venting or gas accumulation sites are demarcated based on the methods of Naudts et al., (2008).

In this study, the backscatter strengths of the area ranges from -26 to -57 dB possessing average backscatter strength of -39.6 dB. A continuous zone of high backscatter is observed in the deeper water (adjacent to the fault trace) where “very high” and “high” seepages are dominant (Figs. 1b and 2). However, in the shallow area, moderate to low backscatter strengths having smooth seafloor topography indicate “moderate” to “very low” seepages. There are two interesting aspects in the acoustic backscatter data. Firstly, backscatter strength gradually increases with the water depth, and later such gradual increment is superimposed by strong transitional gradient of backscatter strength in and around some identified geological features (e.g., fault, pockmarks, small mounds etc.). Occasionally, considerable change of backscatter strength (abruptly high) is also observed in some patches especially in the shallower side of the study area which seems to be featureless in terms of bathymetry. Continuous zone of high backscatter return may refer to the extension of the active seepages over the area and maximum backscatter strength nearby the pockmarks (Feng et al.,

2010). These are clearly shown in Fig. 3, which indicate maximum seepage accumulation zone. Spreading area of the concerned seeps extended in their locations even at a reasonable distance from the pockmark centre (Fig. 3). Also, small patches of high backscatter without the presence of pockmarks in the shallower depth exhibit passive seeps over the area. Seepage areas associated with some representative pockmark samples are illustrated in Fig. 3a-d. In the shallower area, low to very low backscatter strength in the surrounding of the seepages are observed (Fig. 3a and b). In the deeper part, surrounding areas have moderate to high backscatter strength (Fig. 3c and d). Moreover, fault scarp (Fig. 3d) triggers the occurrence of diffusive type of seepages over a quite larger area, while it is more concentrated to a smaller part in other areas (Fig. 3a-c). Dashed lines in red and black colors indicate pockmark and seepage area respectively. Fig. 4 represents an overall presentation of (a) pockmark orientation (b) seep orientation, and (c) seep direction from pockmark centre in the study area. Though orientation of pockmarks is unimodal (NNW-SSE) but orientation of seeps is bimodal (Fig. 4b). Besides, more than 90% seeps are located in the eastern flank of the pockmarks (Fig. 4c), which is also an important aspect in this seepage area. In our study, location of maximum relief inside the pockmarks is termed as pockmark centre and site of maximum backscatter strength associated with respective pockmarks is termed as seep centre or maximum gas accumulation zone. Visual observations and measurements of the features were made using 'ArcGIS' tools.

2.4 Fractal dimension estimations

In order to quantify the seafloor seepage pattern in terms of backscatter intensity we have employed fractal techniques. Accordingly, the whole study area is divided into several small units (i.e., small boxes). Initially, high resolution black & white backscatter image was saved in bitmap (*.bmp) format and then gridded regularly by 400 x 400 pixels (500 x 500 m), dividing the whole area into 398 boxes (Fig. 2) having equal shape and sizes. Then, the box images are used in Benoit 1.3 fractal analysis software (developed by Trusoft Inc.) for calculating fractal such as box dimension (D_{box}), which is expressed as: $N(d) \approx 1/d^{Dbox}$ (Zamora-Castro et al., 2008), where 'N (d)' is the number of boxes having size (d) necessary to cover the fractal object in a two dimensional backscatter image plane. In the Benoit, the input image size defines both the side-length of largest box and the coefficient of box size decrease. Here side-length of largest box was 100 pixels, coefficient of box size decrease was 1.3, and number of box sizes was 18. Also, information (D_{info}) dimension is computed as: $I(d) \approx - D_{info} * \log(d)$ (Seuront, 2010), where I(d) denotes the information entropy. In Benoit, default input parameters are used while calculating fractal dimensions. For self-similar fractal dimension estimation using Benoit, the program first converts gray tone images (pixel

values range from 0 to 255 digital numbers) into binary one i.e., black and white images. To perform this conversion, a threshold is used by the software. The default value of threshold is 128 (digital number). Therefore, Benoit software can calculate fractal dimension at a single scale, and its self-similar characteristics such as: box and information dimensions of a monofractal sets are estimated for 398 blocks. Moreover, due to the self-affine nature of the bathymetric profiles (Goff and Jordan, 1989; Malinverno, 1990; Kraft and de Moustier, 2010), fractal dimensions are calculated from a set of equally spaced N-S trending profiles. Firstly, Hurst exponent ($H_{R/S}$) of these profiles is calculated using R/S method. R/S (w) is the self-rescaled self-adjusted range. The basis of the method is that, because of the self-affinity, the range taken by the values of the input profile in a window of length w is expected to be proportional to the window length to a power equal to Hurst exponent i.e. $R/S(w) = w^H$ (Seuront, 2010). If the trace is self affine, the plot will follow a straight line whose slope would equal to Hurst exponent. Then the fractal dimension ($D_{R/S}$) is computed using Hurst exponent: ($D_{R/S} = 2 - H_{R/S}$) employing Benoit.

3. Results and discussions

3.1 Fractal dimension to characterize the seafloor

Fractal analyses have been performed for each block converting gray tone images to binary one, which results in an area with a very high backscattering strength/seepages having higher fractal dimension (Table 1). The estimated fractal dimensions for both the methods such as D_{box} and D_{info} shows very high correlation coefficient (0.97) for 398 blocks (Fig. 2). The fractal dimensions (D_{box}) are found to be within the range of 1.00-1.95. It is also observed that the area having higher backscatter strength shows higher fractal dimensions and vice versa. Moreover, association of higher fractal dimension in the dominant pockmarks areas are also worth mentioning here. We have classified the study area into six different seepage zones (Tables 1 and 2) based on the estimated fractal parameters, viz. i) "very high" seepage zone (mean D_{box}= 1.95), comprising 71 blocks, and having approximate area of 17.4 km^2, ii) "high seepage" zone (mean D_{box}= 1.93), comprising 93 blocks, and having approximate area of 22.8 km^2, iii) "moderate seepage" zone (mean D_{box}= 1.85), comprising 81 blocks and having approximate area of 19.9 km^2, iv) "low seepage" zone (mean D_{box}= 1.73), comprising 67 blocks and having approximate area of 16.4 km^2, v) "very low" seepage zone (mean D_{box}= 1.48), comprising 33 blocks, and having approximate area of 8.1 km^2, and vi) 'no seepage zone' (D_{box} values cannot be computed), comprising 53 blocks, and having approximate area of 13.0 km^2.

Fractal dimensions ($D_{R/S}$) of bathymetric profiles vary between 1.83 and 1.19. No correlation between the fractal dimensions of the bathymetry and backscatter is made as used datasets are dissimilar in nature. However, a general trend noticed for the profiles having lower fractal dimensions ($D_{R/S}$) where corresponding values of the box/information dimension (D_{box} / D_{info}) for the same blocks are relatively higher. In Table 1, box pattern of backscatter image blocks, bathymetry contours of six represented samples are shown. Estimated fractal dimensions of these blocks are also given in Table 2. Input image details and default parameters in Benoit are also given (Table 2). While comparing the results, we noticed that there is a greater consistency between the box and information dimensions (estimated from backscatter imagery) than the roughness-length method (estimated from bathymetric profiles). Our classification and characterization of entire study area based on fractal parameters involves the degree of roughness of the area i.e., seafloor seepage pattern. We have considered one block of each seepage groups for further analyses and unraveling the seepage pattern in the area. Hence, six representative seepage blocks were chosen and numbered as: F20, J19, F07, Q19, S23 and N25 having 'very high', 'high', 'moderate', 'low', 'very low', and 'no evidence' of seepages respectively (Fig. 2). The characteristics of these blocks along with the representative images are already shown in Table 1.

3.2 Identifying seafloor seepages using backscatter data

Fig. 5a shows that the number of pockmarks (in percentages) in "very high" and "high" seepage blocks are 35.2 and 32.4 respectively. The percentages of the pockmark numbers are decreasing according to the seepage types. In general, circular and elliptical pockmarks are dominant in "very high" seepage area. But significant number of elliptical and elongated pockmarks are also observed for "high' and "moderate" seepage areas. The elliptical and elongated pockmarks in the "high" seepage area are greater than the circular pockmarks. Though, "very high" seepage area possessess maximum circular pockmarks but total number of pockmarks are less than the "high" seepage area (Fig. 5b). Fig. 5c shows frequency distribution plot of the normalized backscattering strengths with respect to the entire seepage area. Normalized backscattering strengths are generally higher for "very high" and "high" seepage areas, which might be due to their proximity to the fault structure.

Pockmark seepages have an important influence on the seafloor geology, especially due to diagenesis of sediments (Hovland and Judd, 1988). Precipitation of diagenetic minerals mainly of calcium and magnesium carbonates are found in the seep site (Behrens, 1988). It has been shown that $CaCO_3$ due to the seepages was formed through CO_2 generated by microbial degradation of the pockmark related gas/fluids. An important consequence of secondary $CaCO_3$ precipitation and

cementation is the reduction of porosity of the seafloor sediment (Buerk et al., 2010). A negative correlation between the sediment porosity and $CaCO_3$ content from biodegradation areas are well known (Wen and Sinding-Larsen, 1996) i.e., due to the low porosity, higher backscatter strength is expected. Therefore, the gray level tone of the multi-beam backscatter data as evident in our study can be related to the seepages where pockmark related environments are dominant (Dandapath et al., 2010).

Some of the backscatter image attributes (Pearson and Gardner, 1997) were found to reduce the uncertainities in seepage prediction in hydrocarbon dominated area (Naudts et al., 2008). Fig. 6 represents the relationship between the multibeam backscatter strength and seepages. We have selected two sample blocks viz, F07 (moderate seepage) and N25 (no seepage) areas. The backscatter images (*bmp) of the areas help to generate histograms and normalized cumulative probability density function plots (Fig. 6a and b) in terms of digital numbers. The histograms (Fig. 6a), of "moderate seepage" (F07) and "no-seepage" (N25) blocks show different distributions indicating nearly Gaussian distribution for 'N25' than the skewed distribution for seepage area 'F07'. These attributes establish that the high digital numbers (backscatter strength) represent seepages of gas/fluids, and low digital numbers indicate no seepages. The semivariogram plots (Fig. 6c and d) show larger variability for seepage area (F07) than the no-seep (N25) area. In 'moderate seepage' area (F07), higher semivariogram values indicate larger variability in backscatter strength due to seeps of gas/ fluids than the block 'N25'. Based on our study we surmise that the multibeam backscatter images can appropriately be used as a reconnaissance tool for pockmark related seep site investigations.

3.3 Self Organized Criticality (SOC) for seepage seafloor setting characterization

In order to describe the behavior of a sand pile, the term "self-organized criticality" (SOC) was adapted (Bak et al., 1987; Turcotte, 1999). While the pile is flat, there is a limited interaction between the different regions of the pile. By adding grains, the pile grows and affecting other grains, thus avalanches of grains occur. The slope of the pile grows until the "angle of repose" is reached. It is the critical state (stationary distribution) due to the impact of gravity. Self-organized structures can be described as fractal structures (Bak et al., 1988) because their properties can be characterized through power laws (Mandelbrot, 1989). The flowchart (Fig. 7) describes the different steps of patch intensity i.e., seepage concentration method to get the scaling exponent 'φ' and threshold concentrations 'c' which characterize the self-organized criticality (SOC).

Seafloor backscatter values between -57 dB and -26 dB were converted to pixel values between 0 and 255. We define the probability Pr ($C \geq c$) as the number of pixels in the gray tone

image blocks for which the value is above or equal to a given threshold value (c). Repeating this process for different thresholds in increasing orders (varying digital numbers at the intervals of 5), the log-log plots of Pr ($C \geq c$) versus c is presented for six representative blocks (Fig. 8). These curves can be fragmented in two sections, the constant part where the increasing seepage concentrations have no impact on the image probabilities (all pixel values are lower than the threshold), and the second part where the probability starts decreasing with a linear trend. Linear regressions on this second part of the curves allow us to get the scaling exponent Φ, which describes the probability distribution [$\Pr (C \geq c) \sim c^{-\Phi}$]. Therefore, using seepage concentrations an estimate of the power law parameters are obtained.

For the first two blocks 'F20' and 'J19', the scaling exponents are $\Phi = 4.35$ and $\Phi = 5.77$ respectively (Table 3). These exponents show the status of the slopes under the seepage effect. It is noted that the exponent increases with decrease in the patch intensity or seepage concentration. The highest scaling exponent ($\Phi = 15.41$) for "N25' block reveals no evidence of seepage. For every block, dynamic balance of seepages predictably operates after reaching their critical state. The high seepage type seafloor represents higher backscatter strength due to the presence of emanated gas/fluids spread over the sediments, and might be surrounded by the pockmarks. As the seepages of gas/fluids increase, the density of gas/fluid in gas charged sediments develops stress towards the critical state. In supercritical state, the avalanches (i.e. the dissipation of gas/fluids) may exert dynamic balance in the system, which is indicated as the SOC in seepage dynamic system. It is evident (Fig. 8) that the decrease in the number of seepage related patches ($\Pr (C \geq c)$) above a critical state is due to the combined effect of both endogenous (i.e., seepage rate, underlying crustal geology, several geological features etc) and exogenous (i.e., seafloor topography, morphology of pockmarks, sediment quality, sliding of pockmarks wall by generating friction by gas bubbles, bottom currents and turbidity etc) processes and/or materials. These sedimentological patterns behave quite significantly in tune with the fluctuations in seepage/patch density. In this pockmark dominated area, representative sample blocks showing set of observations with different values of c and Φ (Table 3) vary due to the seepages (blocks: F20 to N25). Further, block N25 shows SOC (c and Φ) having higher slope because of negligible seepage, whereas in other blocks the SOC decreases according to its seepage intensity. However, for block N25 having low backscatter strength with no seepage (the non- existence of pockmarks over the area) also indicate inability of the sediments to trap gas emanated from the adjacent pockmarks. Besides, we attribute such a low SOC (c and Φ) for N25 block due to an evidence of sediment cover over the seepage material formed as a consequence of monsoon-related sediment movement (Shetye et al., 1990) (Table 3).

In this study area, we observed that the "very high seepage" (F20) block exists along the faulted region where maximum pockmarks are situated (Figs. 1b and 2). Due to the existence of the fault, the bottom topography is rough along with the backscatter strength. Higher roughness indicate higher fractal dimension (i.e. the rough, fragmented, space-filling seepage distributions). Whereas, for blocks (J19) around the "high seepage" (Fig. 2), the topography (Table 2) is comparatively smoother, therefore, showing the low fractal dimension (Table 1). In the shallower areas i.e., below 210 m isobaths, the area is characterized with "moderate" (F07) seepage due to moderate pockmark numbers (though less than the "very high" and "high" seepage areas). Towards the further shallower part, the blocks such as "low seepage" (Q19) and "very low seepage" (S23) possess limited occurrence of pockmarks, and strong affect of monsoon bottom currents from shelf (than the areas towards the slope) (Dandapath et al., 2010). As a result of these two diverse phenomena, study blocks become comparatively smooth in topography. Further, bottom currents promote transportation of the sediments and deposit over gas-charged/seepage sediments (Rollet et al., 2009), which in turn indicating a significantly low fractal dimensions.

3.4 Application of multifractality due to seafloor seepage

In order to understand the mutifractality of the seafloor seepage, we have adopted Seuront and Spilmont (2002) method. Traditional estimation of the fractal dimension for multiple processess may provide single fractal dimension indicating single process rather than the multiple ones as explained by Mandelbrot (1989). Unlike fractal analysis, the multifractal analysis provides idea about the functionality of the associated parameters (Halley et al., 2004) to understand the related processess. Present study block considered as a space distribution of different pixel concentrations. After applying a threshold to the concentration, gray tone images were transformed into binary ones. For this, the fractal dimension using box dimension (D_{box}) method is calculated. And this method is repeated for different thresholds in digital numbers starting from 40 to 255 at an interval of 12, and obtained plots of the multifractal functions (Fig. 9) for six chosen blocks. Using different thresholds, the two dimensional distribution can be divided into a series of black and white patterns. In white areas the seepage exceeds the given threshold and in black area it is empty. Each concentration threshold of a particular block can be related to one fractal dimension, which ultimately resulted in a multifractal function (Seuront, 2010) with respect to the different seepage concentrations. The multifractal behavior of "very high" to "no evidence" of seepages (i.e., six blocks) are presented in Fig. 10. This figure shows multifractal characteristics for backscatter images i.e., the fractal dimension change according to the concentration thresholds. Moreover, it can be observed that our estimated box dimension (D_{box}) values for the six blocks are matching (Fig. 10) well for selected

threshold value of 128 (default value of the Benoit algorithm) while estimating fractal dimension of the six representative blocks (Tables 1 and 2). It is observed that the fractal dimensions decrease as the seepage concentration increase for a particular seepage block. The degree of reduction in fractal dimensions are also function of the basic characteristics of the seafloor nature and influence of other associated parameters like topography and sediment movement due to bottom currents etc. For "very high" (F20) and 'high' (J19) seepage areas, the fractal dimensions are generally higher, however, they also show characteristic decline in the fractal dimensions as the concentration increases. The degree in reduction of the fractal dimensions with respect to the seepage concentration become higher as the seepage concentration increases for "moderate" to "very low" seepage blocks (F07 to S23). The seepage concentrations smoothens the seafloor. This increase in seafloor smoothness or fall in fractal dimension may also be related to the transported coarse sediment from the shelf due to the monsoonal related bottom currents or slumping of the seafloor materials lying adjacent to the outer slope. However, for rough i.e., fragmented and space-filling blocks (F20, J19) the degree of increase in the smoothness is lower than the "moderately rough" to "very low" seafloor blocks (F07 to S23). Due to the scarcity of temporal data, it is difficult to prove the temporal fluctuations of the pockmark seepages from present study area. However, the presented multifractal characteristics of six seepage blocks provide an evidence of the pockmark related processes.

4. Conclusions

Present investigation reveals that the variable seafloor backscatter strength is related to the estimated fractal dimensions. Estimated fractal dimensions such as: box (D_{box}) and information (D_{info}) for 398 blocks display 97% correlation. The seafloor roughness is grouped into six classes depending on the fractal dimensions. Besides, we also infer that nearly 70 % of the area is dominated with gas-charged sediments (Dandapath et al., 2010). The seepages are concentrated densely along the fault trace in deeper waters, while the sparsely located seepages in the shallower depths indicating transportation of surface sediments due to the routine monsoonal currents. High backscatter strength including rough topography along the upper slope of the pockmark region reflects multifractal behavior of seepage distribution which in turn reveals higher fractal dimensions. However, characteristics of the areas without/limited seepages having smooth/moderately rough seafloor show low fractal dimension i.e., less significant non-linear behavior.

Present investigation also suggests patchy seepage patterns signifying the intermittent fluctuations in non-equilibrium systems. We presume that the combined results of processes like nature of pockmarks, fault trace, sediment type, slumping of pockmark's wall, sediment movement

due to bottom current control the dynamic balance in seepage system, which in turn appear to be similar to the sand pile model. The self organizing criticality (SOC) parameters are represented as concentration thresholds (c) and exponents (Φ) for representative six seepage blocks. In the study area, negligible seepage block shows highest exponent (Φ) indicating poor seepage scatter, whereas, for remaining blocks the exponent value decreases as the seafloor seepage increases. The "very high seepage" block exists along the faulted region where maximum pockmark scattered having the highest threshold and the low exponent parameter. This low value indicates gentle slope, in turn, showing addition of further seepage concentrations having limited change in probability of the concentration than the higher exponent for low seepage blocks. Thus, our study emphasizing the multifractal behavior of seepage blocks clearly depicts the different characteristics of the function (D_{box}) for chosen seepage blocks. Hence, we conclude that the differences of their multifractal shapes characterize the typical nature of seepages.

Acknowledgements

We acknowledge Dr. S. R. Shetye, Director, NIO, for his kind permission to publish this work. The data acquisition was carried out under the "Exclusive Economic Zone mapping program" (GAP 2002) of the Ministry of Earth Sciences (MoES), New Delhi, while the relevant interpretation was completed under the "Ocean Acoustic Program" (GAP 2248) of National Institute of Ocean Technology (NIOT), Chennai (MoES) respectively. We also thankfully acknowledge Prof. K. N. Prudhvi Raju for his guidance. SD and DG acknowledges financial support from CSIR NET fellowship. We place on record our thanks to the two anonymous reviewers for their thought provoking and meticulous corrections which improved our manuscript. Our thanks are also due to the Editor for his encouraging words and suggestion for the quick submission of revised manuscript. This is NIO contribution no. xxxx.

References

Abrams, M.A., 1996. Distribution of subsurface hydrocarbon seepage in near-surface marine sediments. In: Schumacher, D., Abrams, M.A. (Eds.), Hydrocarbon Migration and its Near-surface Expression. AAPG Memoir 66, pp. 1–14.

Andrews, B.D., Brothers, L.L., Barnhardt, W.A., 2010. Automated feature extraction and spatial organization of seafloor pockmarks, Belfast Bay, Maine, USA. Geomorphology 124, 55–64.

Bak, P., Tang, C., Wiesenfeld, K., 1987. Self-organized criticality: an explanation of the 1/f noise. Phys. Rev. Lett. 59, 381–384.

Bak, P., Tang, C., Wiesenfeld, K., 1988. Self-organized criticality. Phys. Rev. A 38, 364–374.

Behrens, E.W., 1988. Geology of a continental slope oil seep, northern Gulf of Mexico. AAPG Bull. 72, 105–114.

Beyer, A., Chakraborty, B., Schenke, H.W., 2007. Seafloor classification of the mound and channel provinces of the Porcupine Seabight: an application of the multibeam angular backscatter data. Int. J. Earth Sci. 96, 11–20.

Blondel, P., 2009. The Handbook of Sidescan Sonar. Springer-Praxis, Chichester. 316pp.

Buerk, D., Klaucke, I., Sahling, H., Weinrebe, W., 2010. Morpho-acoustic variability of cold seeps on the continental slope offshore Nicaragua: result of fluid flow interaction with sedimentary processes. Mar. Geol. 275, 53–65.

Calvert, S.E., Pedersen, T.F., Naidu, P.D., von Stackelberg, U., 1995. On the organic carbon maximum on the continental slope of the eastern Arabian Sea. J. Mar. Res. 53, 269–296.

Chakraborty, B., Mukhopadhyay, R., Jauhari, P, Mahale, V., Shashikumar, K., Rajesh, M., 2006. Fine-scale analysis of shelf-slope physiography across the western continental margin of India. Geo-Mar. Lett. 26, 114–119.

Chand, S., Rise, L., Ottesen, D., Dolan, M.F.J., Bellec, V., Bøe, R., 2009. Pockmark-like depressions near the Goliat hydrocarbon field, Barents Sea: morphology and genesis. Mar. Petrol. Geol. 26, 1035–1042.

Dandapath, S., Chakraborty, B., Karisiddaiah, S.M., Menezes, A., Ranade, G., Fernandes, W., Naik, D.K., Prudhvi Raju, K.N., 2010. Morphology of pockmarks along the western continental margin of India: employing multibeam bathymetry and backscatter data. Mar. Petrol. Geol. 27, 2107–2117.

Dewangan, P., Ramprasad, T., 2007. Velocity and AVO analysis for the investigation of gas hydrate along a profile in the western continental margin of India. Mar. Geophys. Res. 28, 201–211.

Dimri, V.P., 2005. Fractals in Geophysics and Seismology: an introduction. In: Dimri, V.P. (Ed.), Fractal Behaviour of the Earth System. Springer-Verlag, Berlin, 1–22.

Feng, D., Chen, D., Peckmann, J., Bohrmann, G., 2010. Authigenic carbonates from methane seeps of the northern Congo fan: microbial formation mechanism, Mar. Petrol. Geol. 27, 748–756.

Fernandes, W., Chakraborty, B., 2009. Multi-beam backscatter image data processing techniques employed to EM 1002 system. In: IEEE OES Proceedings of the International Symposium on Ocean Electronics (SYMPOL 2009). Department of Electronics, Cochin University of Science and Technology, Kochi, India, pp. 93–99.

Fox, C.G., Hayes, D.E., 1985, Quantitative methods for analyzing the roughness of the seafloor. Rev. Geophys. 23, 1–48.

Goff, J. A., Jordan T. H., 1988, Stochastic modeling of seafloor morphology: inversion of Sea Beam data for second-order statistics, J. Geophys. Res., 93, 13589-13608.

Halley, J.M., Hartley, S., Kallimanis, A.S., Kunin, W.E., Lennon, J.J., Sgardelis, S.P., 2004. Uses and abuses of fractal methodology in ecology. Ecol. Lett. 7, 254–271.

Hovland, M., Judd, A.G., 1988. Seabed Pockmarks and Seepages: Impact on Geology, Biology and the Marine Environment. Graham & Trotman, London. 293pp.

Hovland, M., Svensen, H., Forsberg, C.F., Johansen, H., Fichler, C., Fosså, J.H., Jonsson, R., Rueslåtten, H., 2005. Complex pockmarks with carbonate-ridges off mid-Norway: products of sediment degassing. Mar. Geol. 218, 191–206.

Kraft, B.J., de Moustier, C., 2010, Detailed Bathymetric Surveys Offshore Santa Rosa Island, Fl: Before and After Hurricane Ivan (September 16, 2004). IEEE J. Ocean. Engg. 35(3) 453-470.

Karisiddaiah, S.M., Veerayya, M., 1994. Methane-bearing shallow gas-charged sediments in the eastern Arabian Sea: a probable source for greenhouse gas. Cont. Shelf Res. 14, 1361–1370.

King, L.H., MacLean, B., 1970. Pockmarks on the Scotian shelf. Geol. Soc. Am. Bull. 81, 3141–3148.

Logan, G.A., Jones, A.T., Kennard, J.M., Ryan, G.J., Rollet, N., 2010. Australian offshore natural hydrocarbon seepage studies, a review and re-evaluation. Mar. Petrol. Geol. 27, 26–45.

Loncke, L., Mascle, J., 2004. Mud volcanoes, gas chimneys, pockmarks and mounds in the Nile deep-sea fan (Eastern Mediterranean): geophysical evidences. Mar. Petrol. Geol. 21, 669–689.

Longley, P.A., Batty, M., 1989. On the fractal measurement of geographical boundaries. Geogr. Anal. 21, 47–67.

Malinverno, A., 1990. A Simple method to estimate the fractal dimension of a self-affine series. Geophys. Res. Lett. 17, 1953–1956.

Mandelbrot, B.B., 1977. Fractals: Form, Chance and Dimension. Freeman, San Francisco. 365pp.

Mandelbrot B.B., 1983. The Fractal Geometry of Nature. Freeman, New York. 468pp.

Mandelbrot, B.B., 1989. Multifractal measures, especially for the geophysicist. Pure Appl. Geophys. 131, 5–42.

Mitchell, N.C., 1991. Improving GLORIA images using Sea Beam data. J. Geophys. Res. 96, 337–351

Mukhopadhyay, R., Rajesh, M., De, S., Chakraborty, B., Jauhari, P., 2008. Structural highs on the western continental slope of India: implications for regional tectonics. Geomorphology 96, 48–61.

Naqvi, S.W.A., Bange, H.W., Farias, L., Monteiro, P.M.S., Scranton, M.I., Zhang, J., 2010. Marine hypoxia/anoxia as a source of CH_4 and N_2O. Biogeosciences 7, 2159–2190.

Naudts, L., Greinert, J., Artemov, Y., Beaubien, S.E., Borowski, C., Batist, M.D., 2008. Anomalous sea-floor backscatter patterns in methane venting areas, Dnepr paleo-delta, NW Black Sea. Mar. Geol. 251, 253–267.

Paropkari, A.L., Babu, C.P., Mascarenhas, A., 1993. New evidence for enhanced preservation of organic carbon in contact with oxygen minimum zone on the western continental slope of India. Mar. Geol. 111, 7–13.

Paull, C., Ussler III, W., Maher, N., Greene, H.G., Rehder, G., Lorenson, T., Lee, H., 2002. Pockmarks of Big Sur, California. Mar. Geol. 181, 323–335.

Pearson, S.M., Gardner, R.H., 1997. Neutral models: useful tools for understanding landscape patterns. In: Bissonette, J.A. (Ed.), Wildlife and Landscape Ecology: Effects of Pattern and Scale. Springer-Verlag, New York, pp. 215–230.

Rollet, N., Logan, G.A., Ryan, G., Judd, A.G., Totterdell, J.M., Glenn, K., Jones, A.T., Kroh, F., Struckmeyer, H.I.M., Kennard, J.M., Earl, K.L., 2009. Shallow gas and fluid migration in the northern Arafura Sea (offshore Northern Australia). Mar. Petrol. Geol. 26, 129–147.

Satyavani, N., Thakur, N.K., Aravind Kumar, N., Reddi, S.I., 2005. Migration of methane at the diapiric structure of the western continental margin of India – insights from seismic data. Mar. Geol. 219, 19–25.

Seuront, L., Spilmont, N., 2002. Self-organized criticality in intertidal microphytobenthos patch patterns. Physica A 313, 513–539.

Seuront L., 2010. Fractals and Multifractals in Ecology and Aquatic Science. CRC Press, New York. 360pp.

Shenoi, S.C., Antony, M.K., 1991, Current measurements over the western continental shelf of India. Cont. Shelf Res. 11, 81–93.

Shetye, S.R., Gouveia, A.D., Shenoi, S.S.C., Sundar, D., Michael, G.S., Almeida, A.M., Santanam, K., 1990. Hydrography and circulation off the west coast of India during the southwest monsoon 1987. J. Mar. Res. 48, 359–378.

Stanley, H.E., Amaral, L.A.N., Goldberger, A.L., Havlin, S., Ivanov, P.Ch., Peng, C.-K., 1999. Statistical physics and physiology: monofractal and multifractal approaches. Physica A 270, 309–324.

Thamban, M., Rao, V.P., Raju, S.V., 1997. Controls on organic carbon distribution in sediments from the eastern Arabian Sea margin. Geo-Mar. Lett. 17, 220–227.

Telesca, L., Lapenna, V., Vallianatos, F., 2002. Monofractal and multifractal approaches in investigating scaling properties in temporal patterns of the 1983–2000 seismicity in the western Corinth graben, Greece. Phys. Earth Planet. In. 131, 63–79.

Turcotte, D.L., 1999. Self-organized criticality. Rep. Prog. Phys. 62, 1377–1429.

Wen, R., Sinding-Larsen, R., 1996. Mapping oil seeps on the seafloor by Gloria side-scan sonar images – A case study from the northern Gulf of Mexico. Nonrenew. Resour. 5, 141–154.

Yun, J.W., Orange, D.L., Field, M.E., 1999. Subsurface gas offshore of northern California and its link to submarine geomorphology. Mar. Geol. 154, 357–368.

Zamora-Castro, S.A., Oleschko, K., Flores, L., Ventura, E. Jr., Parrot., J.F., 2008. Fractal mapping of pore and solid attributes. Vadose Zone J. 7, 473–492.

Ziegler, M., Lourens, L.J., Tuenter, E., Hilgen, F., Reichart, G.-J., Weber, N., 2010. Precession phasing offset between Indian summer monsoon and Arabian Sea productivity linked to changes in Atlantic overturning circulation. Paleoceanography 25, PA3213, doi: 10.1029/2009PA001884.

Figure Captions

Fig. 1: (a) Location of study area including some of the main structural features of the region. On land Dharwarian trend shown as dotted lines (NNW-SSE trending Precambrian orogenic structure). Red highlighted lines and grey shade indicate the identified bottom simulating reflectors (BSR). MSBR refers to Mid-Shelf Basement Ridge, and WCF indicate West Coast Fault. (b) Backscatter map of the study area showing 160 to 320 m isobaths with an interval of 20 m depth. Pockmarks are indicated by crossed circles. Black, blue and red circles with cross marking represent circular, elliptical and elongated pockmarks respectively. Dashed lines indicate location of identified faults. Black arrows show bottom current directions. Solid colored squares represent the sediment types (see legend). Inset shows outline map of western continental margin of India with the location of the part of the Arabian Sea. (based on Dandapath et al., 2010)

(Approximate location: section 1)

Fig. 2: Segmentation and classification map of the study area based on the estimated fractal dimensions (D_{box}) of the 398 sample blocks. Left top corner of the figure provides histograms of the estimated fractal dimensions of the total number of the blocks. Sample study blocks used for detailed study are indicated as squares. Inset shows correlation (r=0.97) between the estimated box and information dimensions of the blocks.

(Approximate location: sub-section 2.3)

Fig. 3: Seepage characteristics associated with some selected pockmarks. Dashed lines in red and black indicate pockmark area and seepage area respectively. Diffusive type of seepage over a large area is observed in the Fig. 3d, while Fig. 3a-c showing concentrated seepage over relatively small area.

(Approximate location: sub-section 2.3)

Fig. 4: (a) Pockmark orientation, (b) seep orientation and (c) seep direction from pockmark centre in the study area.

(Approximate location: sub-section 2.3)

Fig. 5: (a) The number of pockmarks in percentage according to seepage types and their shapes (circular, elliptical and elongated). (b) The area (in percentages) covered by the different seepage types and different pockmarks shape. (c) The normalized backscatter strength in percentages according to seepage types and pockmark shapes in the study area.

(Approximate location: sub-section 3.2)

Fig. 6: (a) Histograms and (b) normalized cumulative probability density functions of the digital number (gray tone image) values from moderate seepage (F07) and non-seepage (N25) blocks. (c) East -west and (d) north- south semivariogram plots of the same blocks are also shown.

(Approximate location: sub-section 3.2)

Fig. 7: The flowchart exhibits the different steps of patch intensity method to get the scaling exponent 'φ' and threshold concentrations 'c' which characterize the self-organized criticality (SOC).

(Approximate location: sub-section 3.3)

Fig. 8: Probability of exceeding given concentration (Pr (C≥c)) (in log) versus concentrations in digital numbers (in log) and backscatter strength dB. Dashed line demarcates the critical concentration (c) with values for every block. The linear regressions show the power law behaviors of the blocks beyond critical concentration. Backscatter strength (dB) and concentration (c) axes are not scaled.

(Approximate location: sub-section 3.3)

Fig. 9: The flowchart illustrates different steps to obtain multifractal function.

(Approximate location: sub-section 3.4)

Fig. 10: The plot between fractal dimensions (D) and patch concentrations in backscattering strength (dB) and digital numbers (0-255) for chosen six sample blocks. For each area the fractal dimensions are computed starting from 40 to 255 (digital numbers) at the interval of 12. Each concentration threshold is related to one fractal dimension, which results in a multifractal structure. The dashed line represents the default threshold (digital number) value 128 used in *Benoit* software.

(Approximate location: sub-section 3.4)

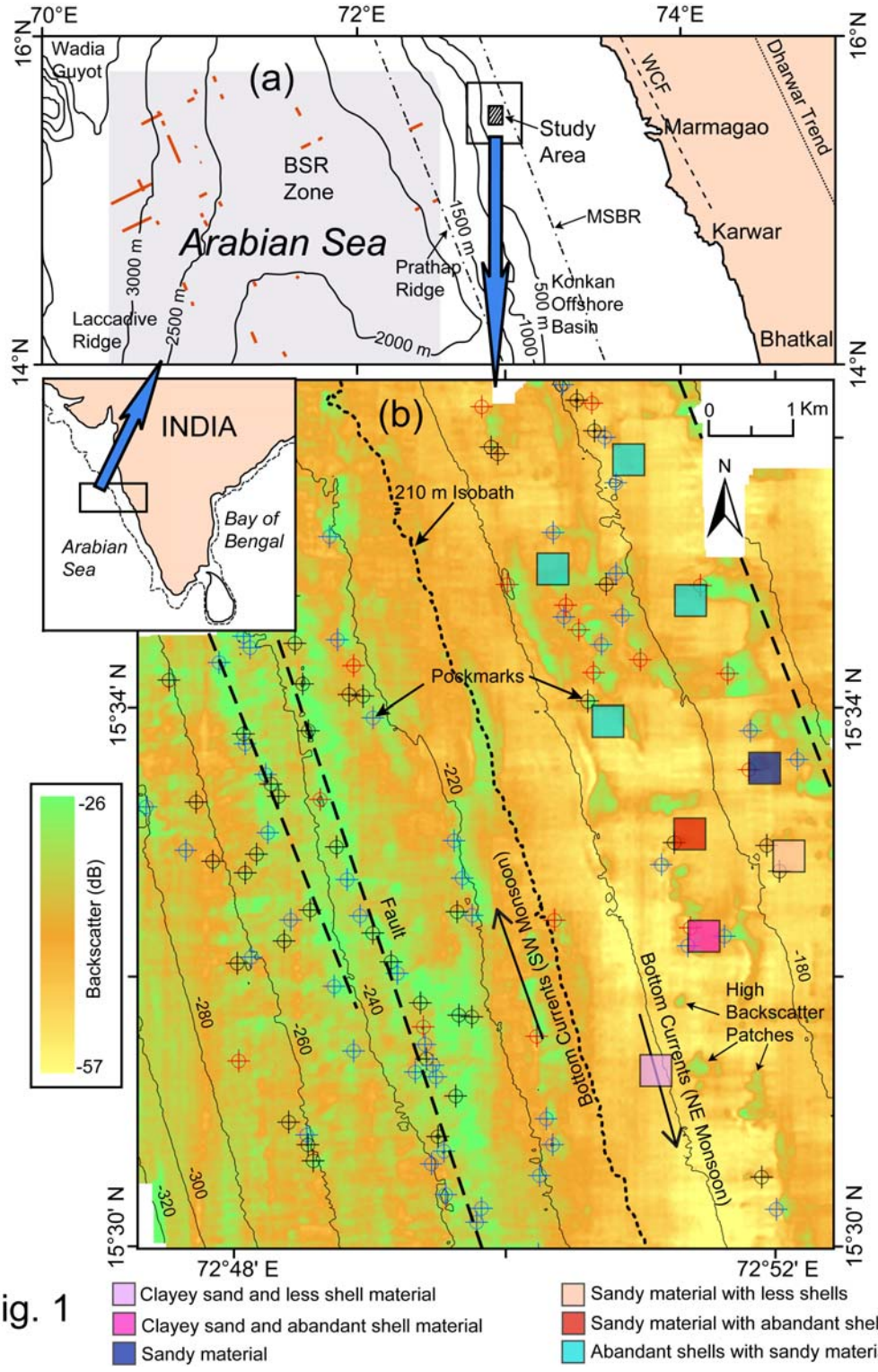
70°E
72°E
74°E
16°N
14°N
Wadia Guyot
(a)
BSR Zone
Arabian Sea
Laccadive Ridge
Prathap Ridge
Study Area
MSBR
Konkan Offshore Basin
Marmagao
Karwar
Bhatkal
WCF
Dhanwar Trend
3000 m
2500 m
2000 m
1500 m
1000
500 m
INDIA
Bay of Bengal
Arabian Sea
(b)
0
1 Km
N
210 m Isobath
Poskmarks
Fault
Bottom Currents (SW Monsoon)
Bottom Currents (NE Monsoon)
High Backscatter Patches
-220
-240
-260
-280
-300
-320
-180
-26
Backscatter (dB)
-57
15°34' N
15°30' N
72°48' E
72°52' E
Clayey sand and less shell material
Clayey sand and abandant shell material
Sandy material
Sandy material with less shells
Sandy material with abandant shells
Abandant shells with sandy material

Fig. 1

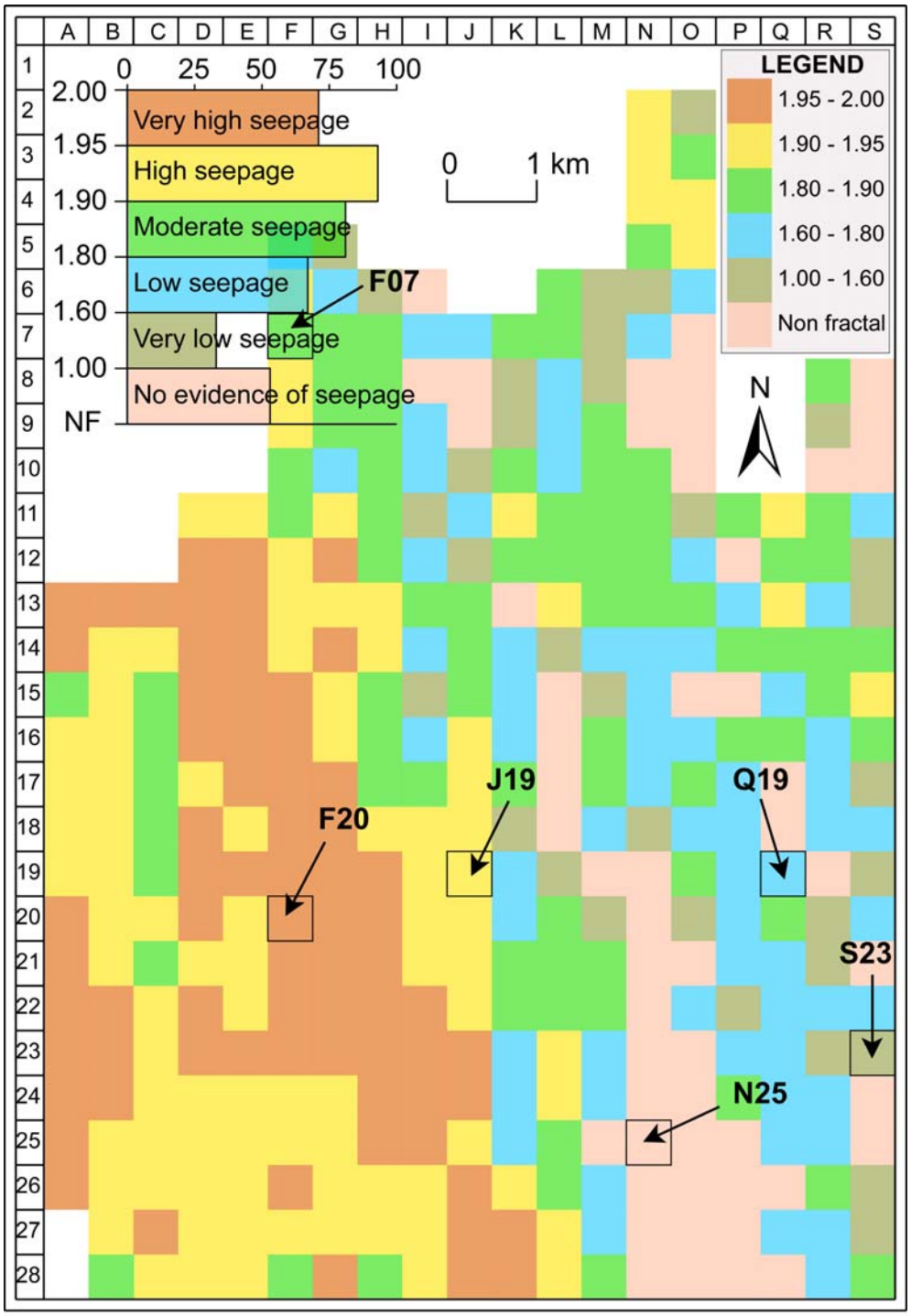

Fig. 2

Sample study blocks

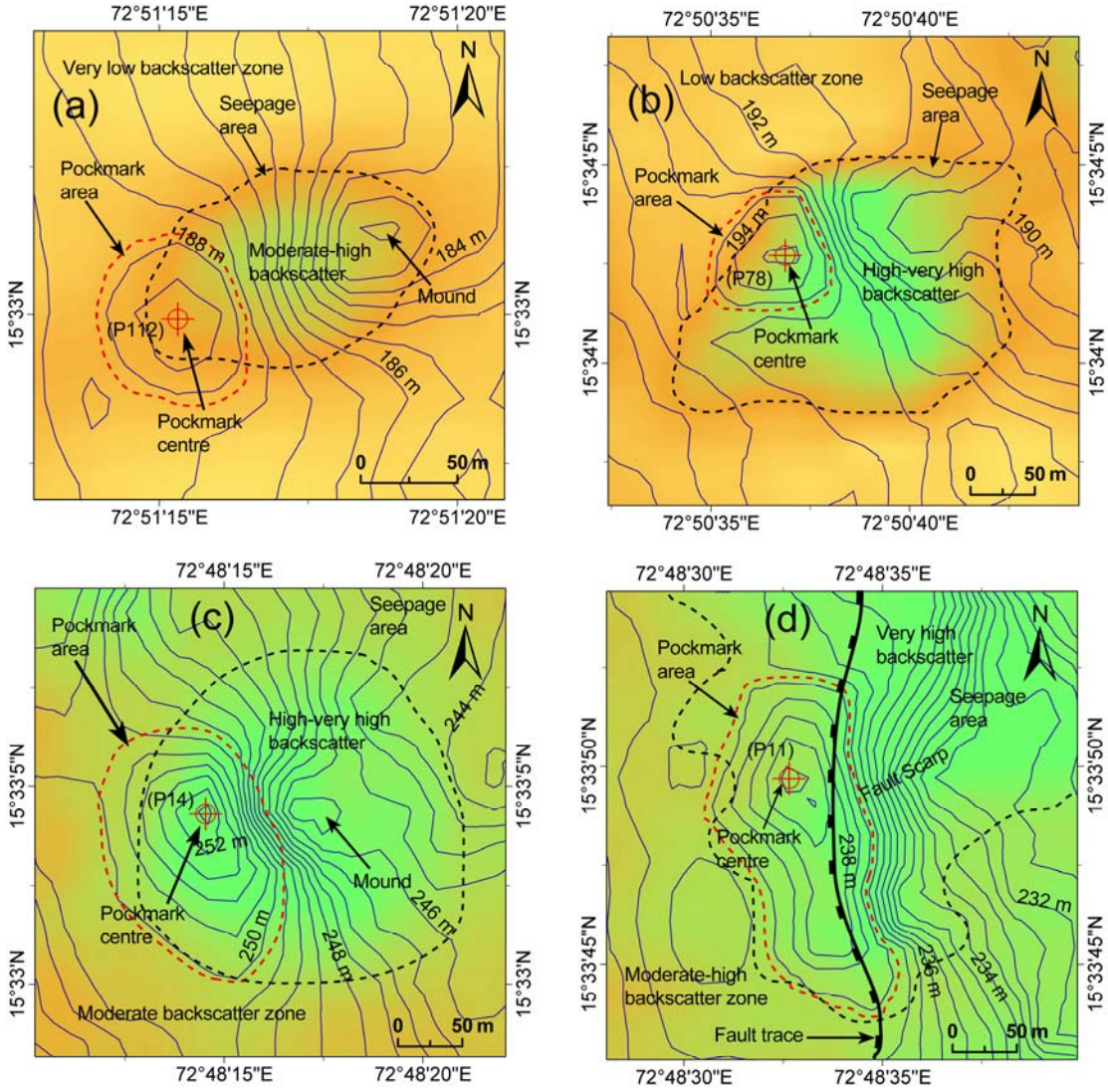
72°51'15"E
72°51'20"E
15°33'N
Very low backscatter zone
(a)
Seepage area
Pockmark area
188 m
Moderate-high backscatter
184 m
Mound
(P112)
186 m
Pockmark centre
0
50 m
N
72°50'35"E
72°50'40"E
15°34'5"N
15°34'N
Low backscatter zone
(b)
192 m
Seepage area
Pockmark area
194 m
190 m
(P78)
High-very high backscatter
Pockmark centre
72°48'15"E
72°48'20"E
15°33'5"N
(c)
Seepage area
Pockmark area
High-very high backscatter
244 m
(P14)
252 m
Mound
246 m
Pockmark centre
250 m
248 m
Moderate backscatter zone
72°48'30"E
72°48'35"E
15°33'50"N
15°33'45"N
(d)
Very high backscatter
Pockmark area
Seepage area
(P11)
Fault Scarp
Pockmark centre
238 m
232 m
Moderate-high backscatter zone
236 m
234 m
Fault trace
Low
High
-57
Backscatter (dB)
-26

Fig. 3

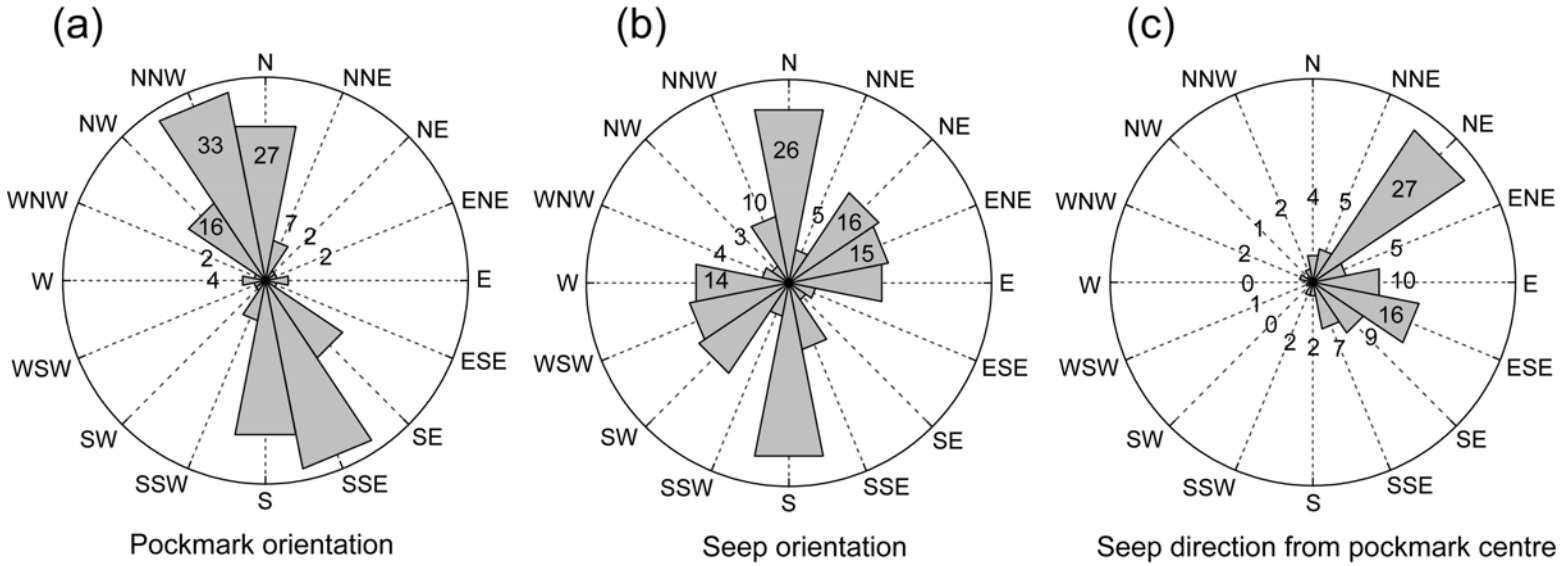
(a)
N
NNE
NE
ENE
E
ESE
SE
SSE
S
SSW
SW
WSW
W
WNW
NW
NNW
33
27
16
7
2
2
2
4
Pockmark orientation
(b)
26
10
5
16
15
3
4
14
Seep orientation
(c)
27
4
5
2
1
2
5
0
10
1
16
0
2
2
7
9
Seep direction from pockmark centre

Fig. 4

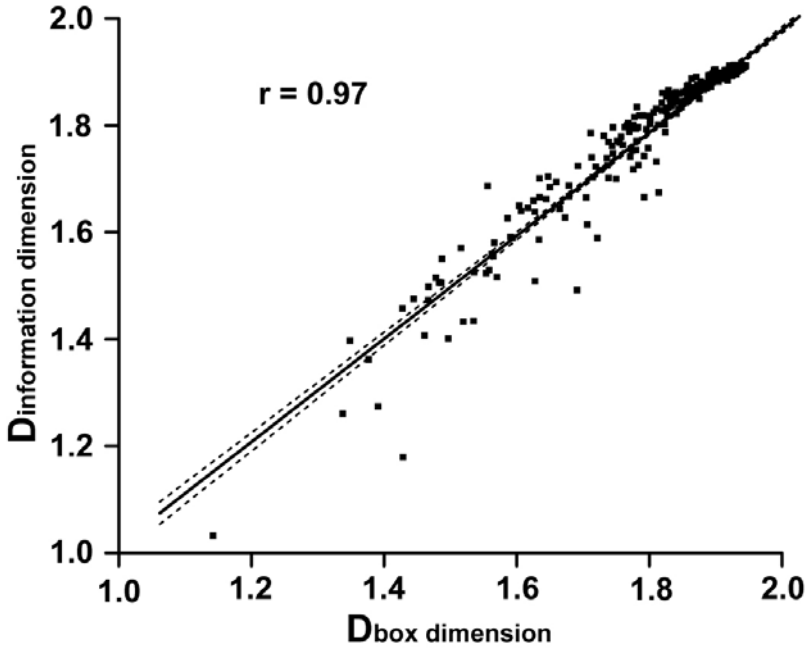
r = 0.97
2.0
1.8
1.6
1.4
1.2
1.0
1.0
1.2
1.4
1.6
1.8
2.0
Dinformation dimension
Dbox dimension

Fig. 5

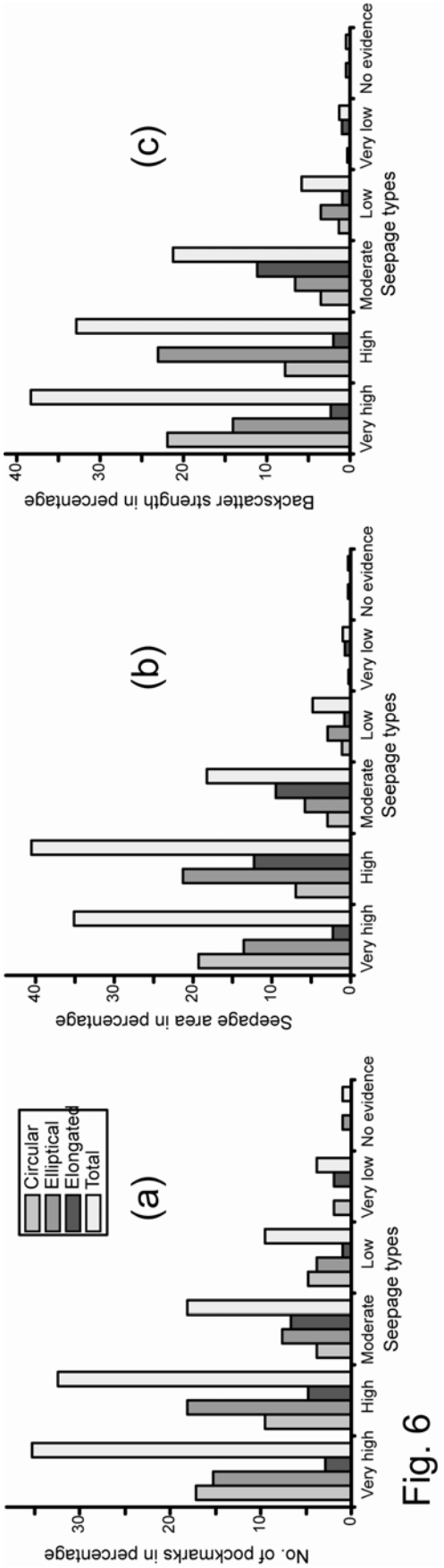
(a)
(b)
(c)
Circular
Elliptical
Elongated
Total
No. of pockmarks in percentage
Seepage area in percentage
Backscatter strength in percentage
Very high
High
Moderate
Low
Very low
No evidence
Seepage types

Fig. 6

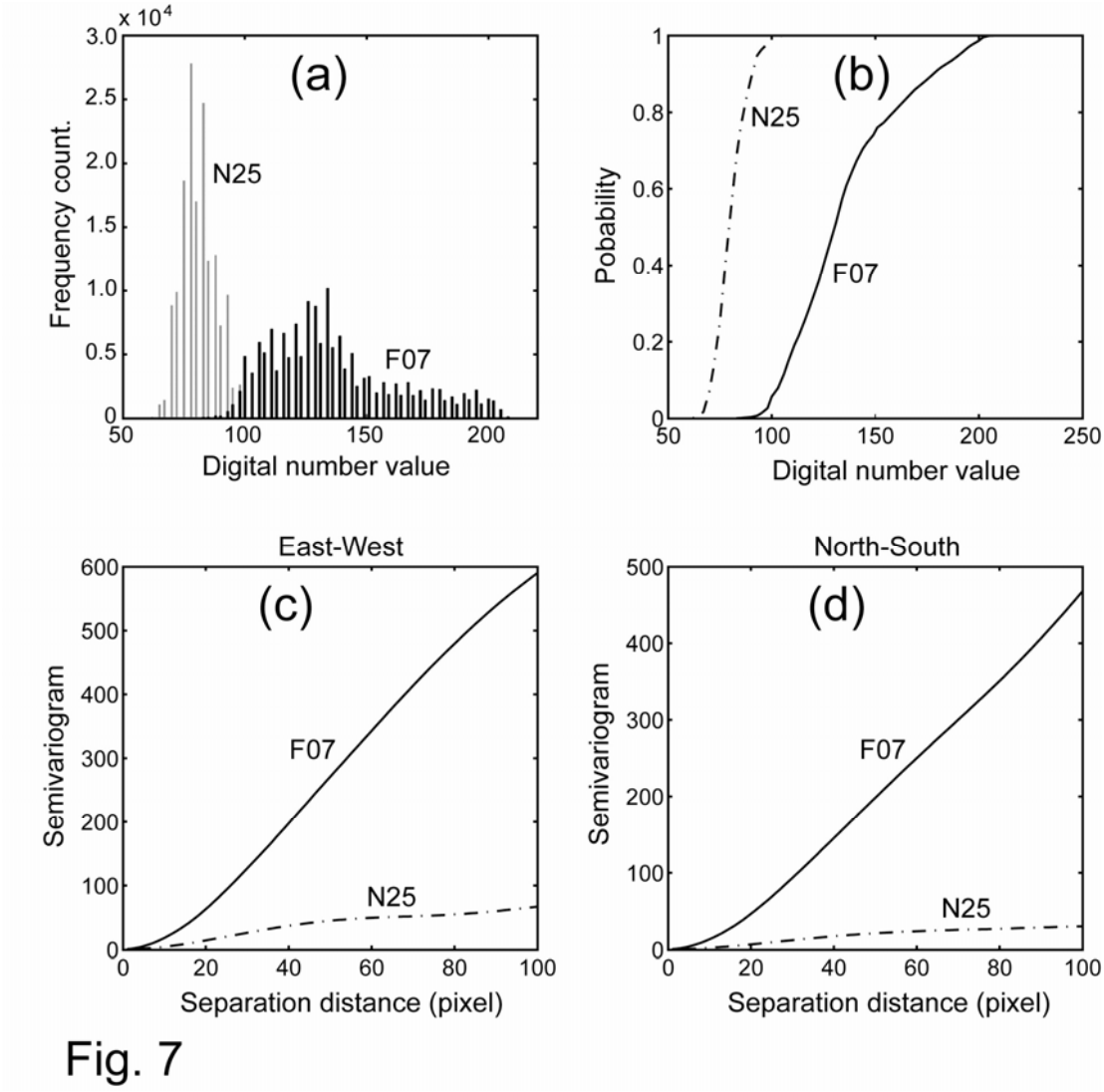
x 10^4
(a)
Frequency count.
N25
F07
Digital number value
(b)
Pobability
N25
F07
Digital number value
East-West
(c)
Semivariogram
F07
N25
Separation distance (pixel)
North-South
(d)
Semivariogram
F07
N25
Separation distance (pixel)

Fig. 7

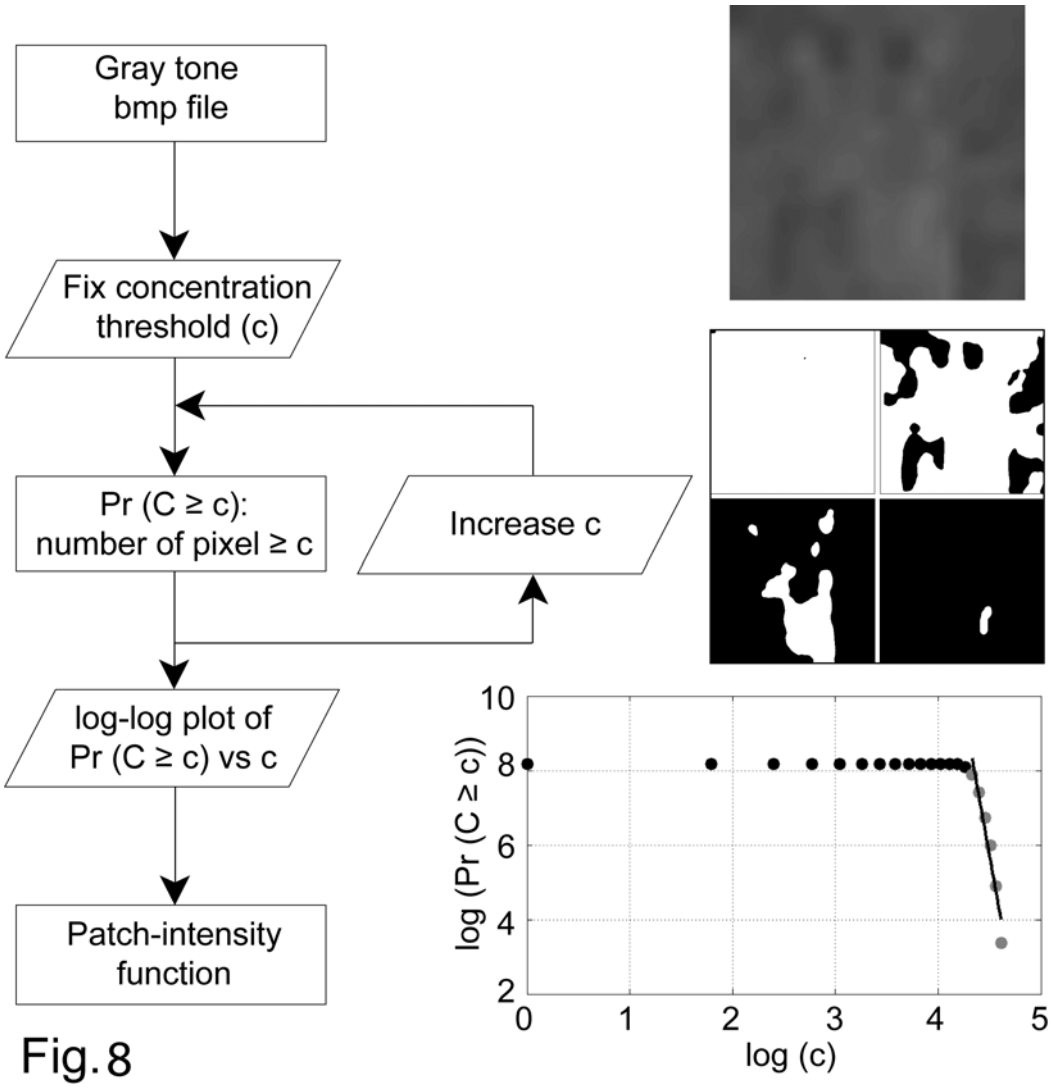
Gray tone
bmp file
Fix concentration
threshold (c)
Pr (C ≥ c):
number of pixel ≥ c
Increase c
log-log plot of
Pr (C ≥ c) vs c
Patch-intensity
function
log (Pr (C ≥ c))
log (c)
10
8
6
4
2
0
1
2
3
4
5

Fig. 8

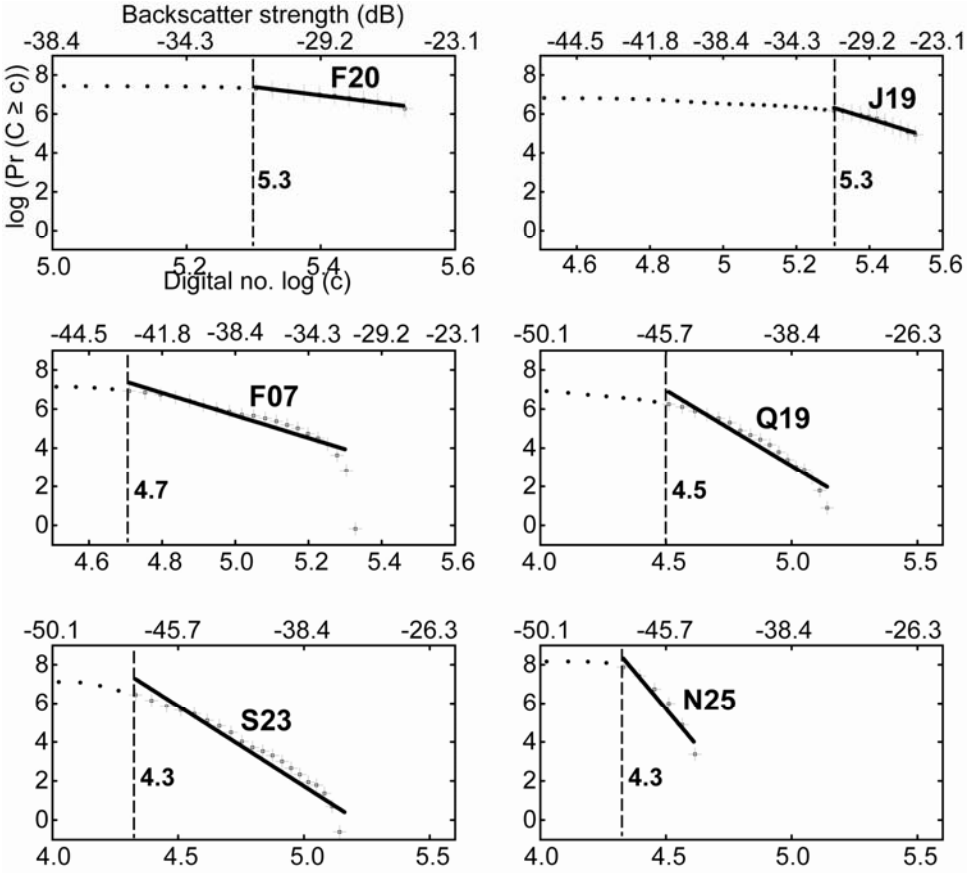
Backscatter strength (dB)
-38.4 -34.3 -29.2 -23.1
log (Pr (C ≥ c))
F20
5.3
5.0 5.2 5.4 5.6
Digital no. log (c)
-44.5 -41.8 -38.4 -34.3 -29.2 -23.1
J19
5.3
4.6 4.8 5 5.2 5.4 5.6
-44.5 -41.8 -38.4 -34.3 -29.2 -23.1
F07
4.7
4.6 4.8 5.0 5.2 5.4 5.6
-50.1 -45.7 -38.4 -26.3
Q19
4.5
4.0 4.5 5.0 5.5
-50.1 -45.7 -38.4 -26.3
S23
4.3
4.0 4.5 5.0 5.5
-50.1 -45.7 -38.4 -26.3
N25
4.3
4.0 4.5 5.0 5.5

Fig. 9

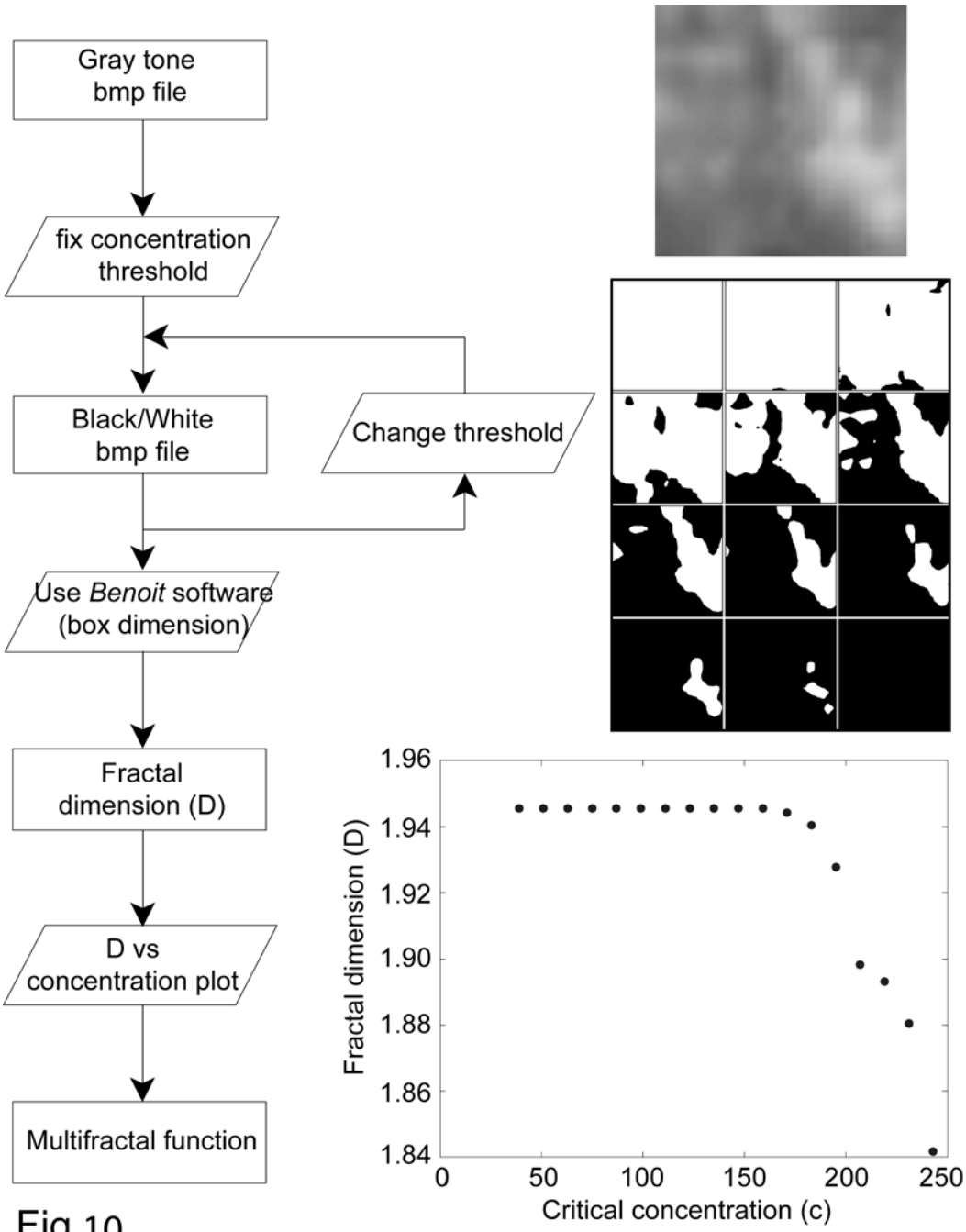
Gray tone bmp file
fix concentration threshold
Black/White bmp file
Change threshold
Use Benoit software (box dimension)
Fractal dimension (D)
D vs concentration plot
Multifractal function
Fractal dimension (D)
Critical concentration (c)
1.96
1.94
1.92
1.90
1.88
1.86
1.84
0
50
100
150
200
250

Fig.10

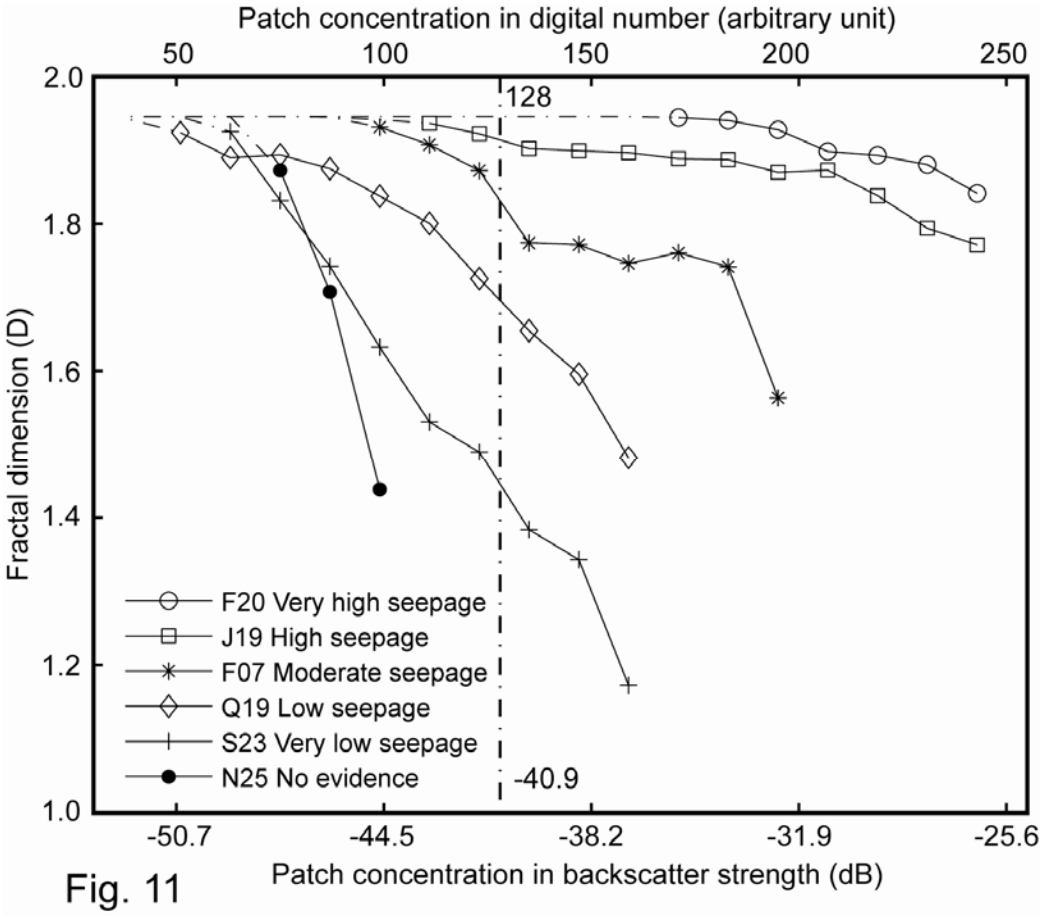
Patch concentration in digital number (arbitrary unit)
50
100
150
200
250
2.0
1.8
1.6
1.4
1.2
1.0
Fractal dimension (D)
128
-40.9
F20 Very high seepage
J19 High seepage
F07 Moderate seepage
Q19 Low seepage
S23 Very low seepage
N25 No evidence
-50.7
-44.5
-38.2
-31.9
-25.6
Patch concentration in backscatter strength (dB)

Fig. 11